

Proceedings of the ASME 2024 International Technical Conference and Exhibition on Packaging and Integration of Electronic and Photonic Microsystems InterPACK2024

October 8-10, 2024, San Jose, California

IPACK2024-141342

ADVANCING IN DATA CENTERS THERMAL MANAGEMENT: EXPERIMENTAL ASSESSMENT OF TWO-PHASE LIQUID COOLING TECHNOLOGY

Ali Heydari NVIDIA Santa Clara, CA Omar Al-Zu'bi Binghamton University Binghamton, NY Yaman Manaserh NVIDIA Binghamton University Santa Clara, CA Binghamton, NY

Russ Tipton VERTIV Columbus, OH Mehrabikermani NVIDIA Santa Clara, CA Jeremy Rodriguez NVIDIA Santa Clara, CA **Bahgat Sammakia**Binghamton University
Binghamton, NY

ABSTRACT

In response to the exponential growth of online platforms and the rise of web-based Artificial Intelligence (AI), the demand for computational power and the expansion of data centers have surged significantly. This trend necessitates advanced cooling strategies and heightened energy efficiency to address the increasing power densities of Information Technology (IT) equipment and the consequent rise in energy consumption. Consequently, there is a significant pivot towards efficient cooling mechanisms that emphasize thermal management and energy efficiency. Against this backdrop, our study thoroughly evaluates a two-phase direct-to-chip liquid cooling system's ability to effectively manage and dissipate heat in high-density rack environments. Central to our research is the deployment of a highly efficient Refrigerant-to-Liquid (R2L) Coolant Distribution Unit (CDU) across multi-racks, which face high thermal demands. This innovative system, featuring an in-row pumped two-phase CDU with a cooling capacity of 160 kW, is intricately integrated with row and rack manifolds and server cooling loops to ensure optimal cooling performance. To accurately simulate the thermal loads encountered in real-world data center operations, the study employs Thermal Testing Vehicles (TTVs). These 3U TTVs are equipped with 2.5 kW heaters, covering an extensive area of 2500 mm², thereby effectively replicating server thermal loads up to 10 kW. The investigation starts with a detailed description of the system's design and continues with the commissioning process. This process includes extensive hydraulic and thermal testing, along with a comprehensive assessment of the impact of pressure drops across the system, focusing on supply manifolds, cooling loops, dry breaks, and return manifolds, utilizing Cooling Loops (CLs)

each containing four Cold Plates (CPs). The study culminates in the analysis of experimental data from heating the TTVs, focusing on the efficiency of two-phase cooling in transferring heat from the TTVs to chilled water using R134a refrigerant as the performance benchmark. Future directions include exploring eco-friendly cooling practices by investigating alternative green refrigerants with low Global Warming Potential (GWP) to replace R134a, aligning with global sustainability goals and the imperative to reduce greenhouse gas emissions. The observed maximum values were calculated at a specific volumetric flow rate of 0.48 LPM/kW and a T_{case} as low as 56.4 °C was achieved. These results demonstrate the system's capability to significantly enhance thermal management in data centers, tackle the challenges presented by high-power density chips, and encourage broader adoption of two-phase cooling technologies as a sustainable strategy for thermal regulation in the face of increasing computational demands.

Keywords: Data center, Thermal management, High heat density, liquid cooling, direct-to-chip, Refrigerants, Two-phase, R2L CDU.

NOMENCLATURE

Q	Volumetric flow rate
q	Power
R_{th}	Thermal resistance
T_{case}	Case temperature
T_{sat}	Saturation temperature
X	Vapor exit quality
ΔP	Pressure drop
ΔP_{CL}	Pressure drop across the cooling le

 $\begin{array}{ll} \Delta P_{return} & Pressure \ drop \ on \ the \ return \ side \\ \Delta P_{supply} & Pressure \ drop \ on \ the \ supply \ side \\ \Delta T_{sub} & Subcooling \ temperature \ at \ the \ CL \ inlet \end{array}$

Abbreviations

CDU Coolant Distribution Unit

CL Cooling Loop CP Cold Plate

CWT Supply Chilled Water Temperature

GWP Global Warming Potential HTC Heat Transfer Coefficient

LPM Liter Per Minute
P2P Pump Two-Phase
PSU Power Supply Unit
QD Quick Disconnect
R2L Refrigerant to Liquid

RST Refrigerant Supply Temperature TIM Thermal Interface Material TTV Thermal Test Vehicle

1. INTRODUCTION

Data centers play a crucial role in our increasingly digital world as the foundation for a vast range of online services, cloud computing, and storage facilities. The need for effective thermal management systems in these data centers has increased significantly due to the rapid growth of data generation and usage. Traditional air cooling systems, that have long formed the foundation of data center thermal management, are struggling to keep up with the increasing power densities of contemporary computing devices [1-3]. In contrast to air cooling, indirect single- or two-phase liquid cooling using microchannel cold plates offers benefits such as reduced system component sizes and increased energy efficiency, owing to the greater heat capacity of liquids [4-8].

Pumped two-phase cooling has been a particularly promising technique in the field of electronics cooling in recent years. The latent heat of the fluid in two-phase cooling allows for more effective heat removal at lower mass flow rates than in single-phase cooling. Additional benefits include higher heat transfer coefficients and more consistent chip temperatures, achieved by operating in the cooling fluid's saturation region [9,10]. In such systems, the refrigerant begins as a liquid, is pumped at a certain pressure, and cycled through a closed loop to heat sinks attached to the electronic components. It absorbs heat from the components before transitioning into a vapor phase, significantly improving its heat-absorption capability over standard single-phase cooling approaches. The vaporized refrigerant is then sent to a heat exchanger condenser, where it is condensed back into a liquid state, ready to begin the cooling cycle again.

For the majority of cooling systems, R134a is the recommended cooling refrigerant because of its well-established reliability, broad availability, and consistent performance

characteristics, Moreover, green refrigerants substitute for R134a would be the next step. Additionally, it has several important benefits over other refrigerants, such as being nontoxic, non-flammable, and non-ozone-depleting, making it a safer overall option. In an experimental investigation, Thiangtham [11] used R134a to study two-phase flow patterns using a multi-microchannel heat sink in the evaporation stage. Lee and Mudawar [12-14] utilized R134a as the working refrigerant for two-phase cooling in electronics applications, achieving impressive thermal performance—up to 840 W/cm² while preventing critical heat flux—at lower saturation temperatures. Bertch [15] examined the effects of using R134a and R245fa on copper microchannel cold plates. Their investigation looked into changes in heat flux, mass flux, saturation temperature and pressure, and vapor quality. The results suggest that the heat transfer coefficient is more susceptible to changes in heat flux and vapor quality, but less to changes in mass flow and saturation pressure. Heydari [16] conducted a thorough analysis of pumped two-phase cooling, examining the impact of various operational aspects on CDU performance and the selection criteria for environmentally friendly refrigerants to replace high-GWP competitors. According to preliminary research, R1234yf appears to be the best substitute for R134a in two-phase rack-level cooling systems. In another study, Heydari [17] proposed a strategy for implementing two-phase cooling at data center IT rack sites when a chilled water source is unavailable by using a refrigerantto-air CDU condenser. Furthermore, Heydari [18] identifies flow nonuniformity in parallel pathways as a significant issue, exacerbated by varying heat loads. The study evaluates two methods—constant flow regulators and flow restrictors—using proof-of-concept cooling loops with ultrasonic flow sensors and 2.5 kW heaters in TTVs. Both solutions demonstrated the ability to significantly reduce flow nonuniformity, with variations as low as 0.15 LPM, using R134a refrigerant, and suggest potential future work with green refrigerants.

This research presents an innovative experimental framework focused on developing and evaluating a two-phase direct-to-chip cold plate liquid cooling system specifically engineered for high-heat-density data centers. The study explores the deployment of a highly efficient in-row R2L CDU with a cooling capacity of 160 kW with a rack level of high thermal demands. System components include row and rack manifolds, cooling loops, TTVs, and facility-chilled water on the CDU's condenser. The research method includes the use of 3U TTVs equipped with 2.5 kW heaters over a 2500 mm² area, simulating thermal loads up to 10 kW. Comprehensive analysis of the system's thermohydraulic performance under various conditions assesses parameters like pressure drops, saturation and subcooled temperatures, vapor exit quality, CP thermal resistance, and heater case temperatures. The findings provide crucial insights into improving cooling solutions in data center infrastructure, with significant implications for the design and operation of future facilities.

2. EXPERIMENTAL SETUP

2.1 System description

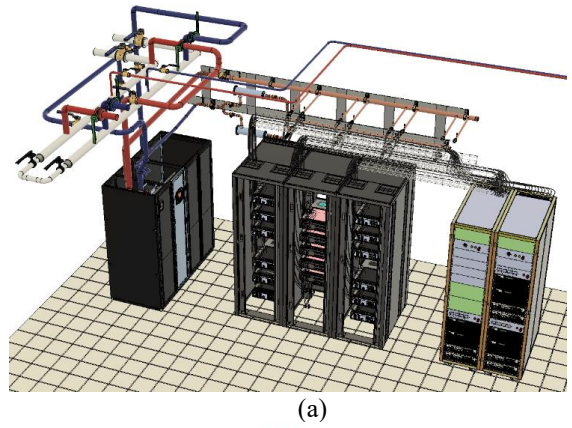
In this system, the experimental setup comprises multiple racks and an in-row R2L CDU that has a cooling capacity of 160 kW, as shown in Fig. 1(a). The two-phase CDU is equipped with pumps that circulate the refrigerant (R-134a) from the condenser to the CLs. The condenser unit dissipates heat from the refrigerant to facility-chilled water. Refrigerant is distributed via custom-designed (row and rack) manifolds to the CLs attached to the TTVs. Each rack contains five CLs, which feature a specialized microchannel cold plate design that supports various flow configurations (parallel, convergent, and split flows) to maximize the heat transfer coefficient in the refrigerant to cool the case temperature of the TTVs through the boiling process. Power supply units generate the necessary power for the TTVs (each equipped with four heaters) to simulate the actual heat dissipation observed in processors.

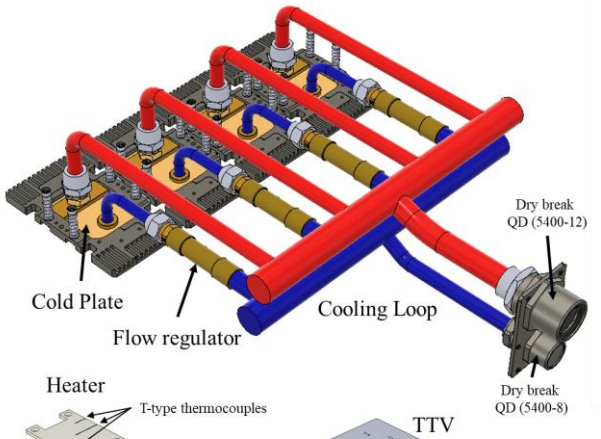
As illustrated in Fig. 2 (a) the sequence of events in the twophase multi-rack system is as follows: Initially, the in-row R2L CDU pumps refrigerant (R-134a) from reservoir tanks to the supply row manifold, which includes two 25-micron filter driers in parallel to prevent moisture and contamination within the system, then distributes the refrigerant to the supply rack manifolds mounted in the racks. From here, the rack manifold branches distribute the refrigerant to each CL, where the flow splits to four parallel CPs in each CL. These CPs use PCM as a TIM and each is attached to a heater to absorb the heat produced by these heaters. After the refrigerant absorbs heat from the TTVs through sensible cooling and latent heat, it exits the cold plates, gathers at the cooling loop outlet, and flows back to the return rack manifold and then to the return row manifold. Subsequently, the two-phase refrigerant re-enters the CDU and flows into the water-cooled condenser. The chilled water, which passes through a 50-micron filter before entering the CDU, is controlled to ensure complete conversion from two-phase flow to sub-cooled refrigerant at a lower temperature to prevent cavitation before the pumps pressurize and recirculate it through the cooling loops, thus repeating the cycle.

Equipped with constant flow regulators, the cooling loops depicted in Fig. 1(b) ensure stable flow in parallel paths under non-uniform heat load conditions through the implementation of two-phase flow control mechanisms. As evaluated by Haydari [18], two types of flow control mechanisms—constant flow regulators and flow restrictors—have been demonstrated to significantly reduce flow nonuniformity, achieving variations as low as 0.15 LPM. Additionally, TTVs, equipped with uniform heat flux heaters, were loaded into racks within a 3U chassis, as illustrated in Fig. 1(b). Chosen for their affordability and suitability, the TTVs mimic real high-heat-density devices and serve as ideal options for assessing the thermal performance of the proposed cooling loops. Each TTV comprises four heaters, each with a surface area of 50 mm × 50 mm and equipped with

three T-type thermocouples to measure the top surface temperature. Capable of reaching a maximum power of 2500 W, or 100 W/cm^2 , the TTVs can achieve a total power level of up to 10 kW.







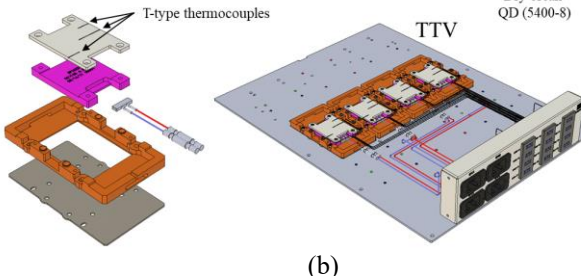


FIGURE 1: The experimental setup used in the study (a) P2P CDU, multi-racks, and PSU (b) TTV and cooling loops characterized in the study.

2.2 Instrumentations

To assess the performance of the system, instrumentation was installed, as depicted in Fig. 2(a). Pressure transducers, thermocouples, and ultrasonic flow sensors were detailed in Table 1 and installed accordingly. Furthermore, Fig. 2(b) displays the instrumented manifolds for supply and return for each CL. For the collection of measured data, a KEYSIGHT DAQ970A was utilized.

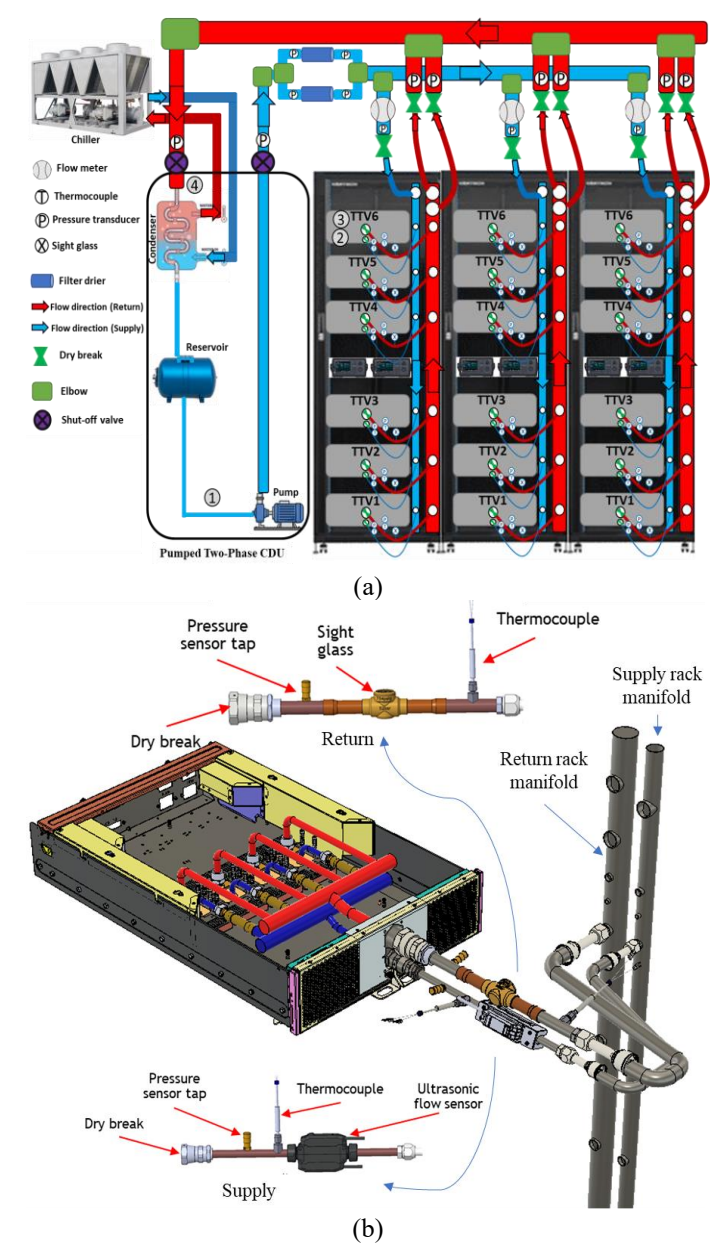


FIGURE 2: (a) Schematic of the proposed system and installed instrumentation. (b) CAD for the instrumented manifolds for supply and return for each CL.

Table 1: Specifications of experimental apparatus

Items	Specification /Description	Accuracy
Pressure transducer	OMEGA PX409-500A10V Inlet and outlet of	±0.08%
Temperature sensor	K-Type, Inlet, and outlet of CLs T-Type, Surface of the Heaters	±0.5°C
Flow sensor	clamp-on micro flow sensor, Inlet of • FD-H32 on the Rack manifolds • FD-X A1 on the CLs	±0.3%
Power supply	KEYSIGHT RP7972A	±0.05%

2.3. Commissioning

The initial commissioning process outlined below follows the system's construction and assembly. When operating with pressurized refrigerants, it is crucial to ensure the system's integrity and leak free. For flushing, the CDU is connected to the row manifold that has two 25-micron external filter driers with replaceable cores on the supply side to enhance filtration as shown in Fig. 3(a), where the row manifold is looped back to itself using hoses as shown in Fig. 3(b).

Initially, the system is pressurized with a small amount of refrigerant (R-134a) and subsequently with nitrogen up to 200 psi. This step is employed to evaluate the system's pressure tolerance and utilizes a modest amount of refrigerant to aid in leak detection via a sniffer, capable of identifying leaked pressurized gases up to 1 ppm. Once the system's integrity is confirmed, a triple vacuum is performed using a vacuum pump to ensure the absence of moisture by reducing the internal pressure to 0.019 psi on the first vacuum. Nitrogen is then purged, followed by a second vacuum, and a second nitrogen purging, then finally, a third vacuum at 0.0085 psi. Subsequently, R-134a refrigerant is gradually introduced and monitored through the sight glass on the CDU reservoirs. In the final step, the pumps are operated for eight hours to flush out any residual debris or contaminants, thereby ensuring the system is clean and ready for operation. The filters are then inspected and replaced with new ones, as depicted in Fig. 3(c) and (d).

After CDU and row manifold flushing is completed, each supply and return branch of the rack manifold is looped back to itself through a manifold equipped with an external 40-micron filter with a replaceable core as shown in Fig. 3(e). This is followed by a triple vacuum and purging with nitrogen until a pressure of 0.0077 psi is reached, after which R-134a refrigerant

is charged. The rack manifold is then connected to the row manifold, and a flushing procedure is performed for 8 hours using the CDU, which connects the CDU, row manifold, and rack manifold. The filters are subsequently inspected as shown in Fig. 3(f) and (g). Finally, after the manifolds with external filters are removed from the rack manifold branches and inspected, the CLs are connected to the rack manifold branches and ready to be tested.



FIGURE 3: (a) Supply manifold 25-micron filter driers with replaceable cores. (b) Row manifold looped to itself by hoses. (c) New filter. (d) The filter after flushing. (e) Manifolds with 40-micron filters are used to loop the rack with itself. (f) New filter. (g) The filter after flushing.

3. GREEN REFRIGERANTS

In response to growing concerns about climate change, a gradual reduction of over 80% in the use of hydrofluorocarbons (HFCs) with high GWP by 2047 has been mandated by the Kigali Amendment to the Montreal Protocol [19,20]. This initiative is supported by the US Environmental Protection Agency (EPA) and the European Union's Directive 517/2014, which impose restrictions on the use of such refrigerants. R134a, a widely used medium-pressure chiller refrigerant known for its high GWP of 1430, is slated for phase-out, prompting the exploration of low GWP alternatives [21].

Viable options such as Hydrofluoroolefins (HFOs), natural refrigerants, and low GWP HFCs have emerged in the search for alternatives [22]. Among these, HFOs like R1234yf, R1234ze (E), and the HFO blend R515B are recognized as suitable substitutes for R134a. These refrigerants are characterized by their low flammability, minimal toxicity, lack of ozone depletion potential (ODP), and very low GWP [23]. Additionally, they are capable of operating under similar conditions to current refrigerants like R134a, thus maintaining efficient performance [24]. A system-level assessment of green refrigerant replacements was conducted by [25], delving into various

operational parameters such as saturation temperature, heat flux, and pressure drop to understand their influence on the system's thermal performance. The research concluded that the suitability of the compared refrigerants for replacement is dependent on various factors, including system size and cost, thereby providing a range of options suited to different data center needs. Consequently, a variety of green refrigerant replacements could be utilized across different systems.

4. RESULTS AND DISCUSSION

To examine the cooling system's performance, a hydraulic and thermal test under defined conditions was performed. In these tests, one rack and five CLs are attached with TTVs.

4.1 Hydraulic test

The hydraulic test of the system was conducted at a constant RST of 22°C, involving the cooling loops and both the supply and return for the row manifold and rack manifold. The test commenced at 20 LPM per rack (4 LPM per CL) and increased to 36 LPM per rack (7.2 LPM per CL). Fig. 4 displays the pressure drop results for the supply and return side of each row manifold and rack manifold at varying flow rates. Great performance is shown by the pressure drop on the row manifold, while the rack manifold expresses a higher pressure drop as the volumetric flow rate increases. It was noted that, since the return side of the rack manifold features larger pipes and QDs than the supply side, the increase in pressure drop was not as significant.

Furthermore, the flow distribution and pressure drop across the CLs, which include dry breaks (QDs; 5400-8 on the inlet and 5400-12 on the outlet), flow regulators, and cold plates, are listed in Table 2. It is noted that a dramatic increase in pressure drop occurs beyond 6 LPM/CL, primarily attributed to the flow regulators. Moreover, Haydai [18] observed that constant flow regulators contribute a pressure drop of 12.2 psi, which is significantly greater than that added by flow restrictors.

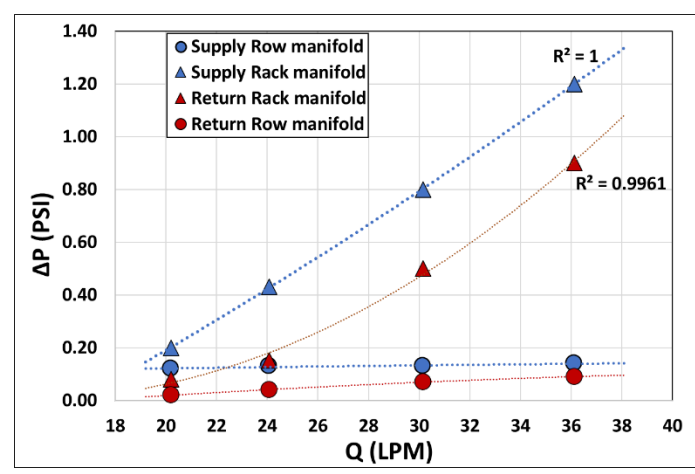


FIGURE 4: Pressure drop across the row manifold and rack manifold at varying flow rates with no heat load.

Table 2: Flow distribution and pressure drop across the CLs at varying flow rates with no heat load.

Q (LPM/ Rack)	CL#	Q (LPM/CL)	ΔP _{CL} (psi)
	CL5	3.67	1.61
	CL4	3.52	1.80
20	CL3	3.89	1.46
	CL2	4.11	1.27
_	CL1	4.85	1.08
	CL5	4.33	2.11
	CL4	4.24	2.30
24	CL3	4.50	1.96
	CL2	4.78	1.77
	CL1	5.44	1.58
	CL5	5.67	3.83
	CL4	5.53	4.03
30	CL3	5.94	3.69
	CL2	6.38	3.50
	CL1	6.59	3.30
•	CL5	6.71	11.22
	CL4	6.67	11.41
36	CL3	7.22	11.07
	CL2	7.62	10.88
	CL1	7.69	10.69

4.2 Thermal test

An experimental setup at the rack level was utilized to characterize various parameters under different heat loads, including the pressure drop, saturation temperature, Delta T subcooling, cold plate thermal resistance, vapor exit quality, and the heater's case temperature. In this test, one (52 U) rack loaded with 5 CLs (Each CL has 4 cold plates with flow regulator) attached using TIM to 5 (3 U) TTVs (each TTV has 4 heaters, 2.5 kW each with an area of 50×50 mm). Table 3 presents the boundary conditions of the thermal test.

Consequently, when the heat load increased while maintaining a constant flow rate, a low pressure drop was observed on both the supply side of the row and rack manifolds, and on the return side of the row manifold. Conversely, on the return side of the rack manifold (from the CL outlet to the inlet of the return row manifold), a heightened pressure drop of 7.6 psi was noted at full heat load, as depicted in Fig. 5. Furthermore, at zero load with the same volumetric flow rate of 24 LPM, the

pressure drop on the return side of the rack manifold was measured at 0.15 psi, as illustrated in Fig. 4. Additionally, Table 4 listed the flow distribution and the pressure drop across the CLs under varying heat loads at a constant flow rate, where the maximum pressure drop reached 4 psi at full thermal load. Importantly, this pressure drop includes the QDs, flow regulator, and CP at the inlet and outlet of the CL.

Table 3: Boundary condition for the thermal test

	BCs
TIM	PTM 7900
q (kW)	10% (5/Rack) (1/TTV) (0.250/heater) 50% (25/Rack) (5/TTV) (1.25/heater) 100% (50/Rack) (10/TTV) (2.5/heater)
Q (LPM)	(24/ Rack) (4.8/ CL)
Fluid	R-134a
RST (C)	24
CWT (C)	8

Moreover, the negative impact on the refrigeration system is attributed to the pressure drop on the return side, as it affects the chilled water temperature required at the CDU. To counteract this pressure drop, refrigerant is often delivered at a higher pressure, noted to be 97 psi at the supply CDU. Consequently, the refrigerant undergoes subcooling at the entrance of the cold plate due to this increased pressure. If the pressure drop on the return side is substantial, excessive subcooling of the refrigerant might occur. This excessive subcooling can adversely affect the thermal performance of the cold plates; specifically, it results in part of the cold plate being cooled with single-phase refrigerant, thereby causing a hot spot to form on the heater, which constitutes the second negative impact. Haydari [16] explored the influence of pressure drop on the return side concerning refrigerant subcooling. According to the study, a considerable amount of sensible heat transfer may be observed, necessitating the definition of an acceptable range for sensible heat percentage. This specified range should be based on the performance of the cold plates, and the system must be designed to function within these established limits. In this study, Fig. 6 displays the impact of the return pressure drop from the CL outlet to the condenser inlet on the subcooled temperature that enters the CL, with varying heat loads and a constant flow rate. As the heat load increases, the pressure drop increases by 4.8 times, which in turn raises the subcooled temperature difference by 2.8 times. Consequently, enhancements such as increasing the pipe size on the return side are suggested to mitigate this pressure drop.

The ΔT_{sub} entering the CLs is influenced by another factor, namely the elevation of the CL. Given that the supply from the rack manifold is positioned at the top of the rack manifold, additional pressure is exerted on the inlet of the CL located at the bottom; (CL1), where it is primarily affected by gravity. Consequently, the T_{sat} for CL1 is affected by this elevation,

where an increase of 2.1 psi in the inlet pressure at this CL is observed. This increase is calculated using the equation (ρgh) , where ρ represents the liquid density, g is the gravitational acceleration constant, and h denotes the elevation of the CL from the supply rack to the CL inlet. As shown in Fig. 7 CL1 has the highest ΔT_{sub} .

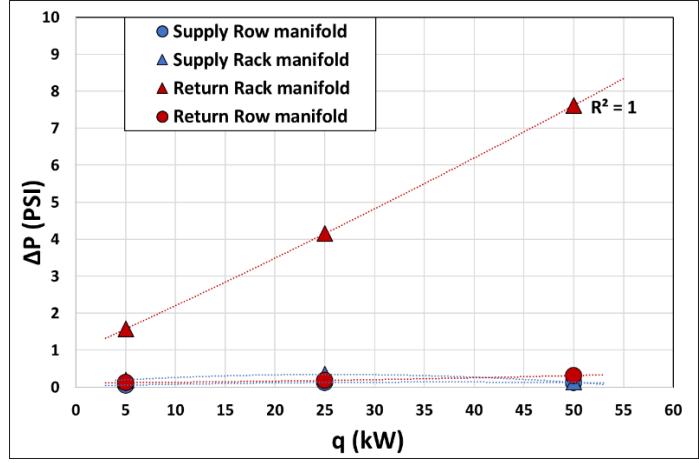


FIGURE 5: Pressure drop across the row manifold and rack manifold at varying heat loads with constant flow rate.

Table 4: Flow distribution and pressure drop across the CLs at varying heat loads with constant flow rate at the supply rack.

q (kW/ Rack)	CL#	Q (LPM/ CL)	$\Delta P_{\rm CL}$ (psi)
	CL5	4.90	1.27
	CL4	4.84	1.48
5	CL3	4.78	1.74
	CL2	4.69	1.75
	CL1	4.60	1.96
	CL5	4.96	1.78
	CL4	4.92	1.97
25	CL3	4.85	2.47
	CL2	4.66	2.56
	CL1	4.53	2.69
	CL5	4.98	3.14
	CL4	4.90	3.42
50	CL3	4.86	3.66
	CL2	4.79	3.81
	CL1	4.57	4.01

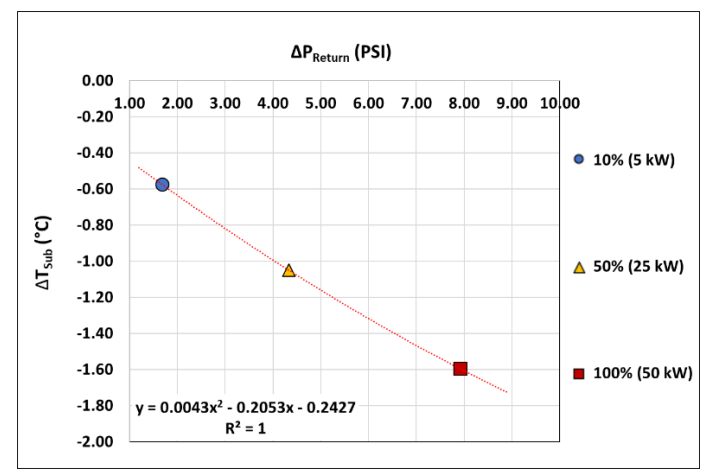


FIGURE 6: The effect of pressure drop of the return side from the CL outlet to the condenser inlet on the subcooled inlet temperature of the CL, with varying heat loads and constant flow rate.

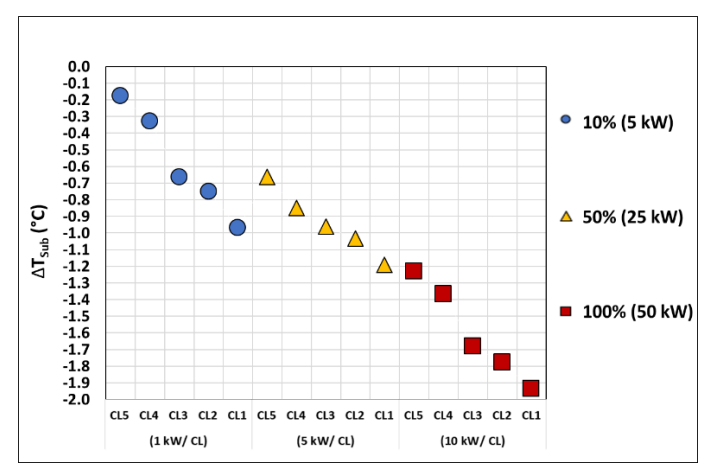


FIGURE 7: The impact of varying heat loads on the subcooled inlet temperature of the CL, with a constant flow rate.

The saturation temperature is influenced by the chilled water source, necessitating adjustments in the refrigerant T_{sat} to maintain the heater case temperature below a specified threshold. This requirement arises when modifications are made to the heater power and CP thermal resistance. Fig. 8 illustrates the maximum case temperatures of the heaters in the TTVs under varying heat loads. Additionally, a peak heater case temperature of 56.4 °C was observed, as shown in Fig. 9. Furthermore, by applying Equation (1) and calculating the thermal resistance, the highest thermal resistance is depicted in Fig. 10; at 250 W/CP, the thermal resistance was found to be higher than at other thermal loads because, at lower heat loads, the percentage of sensible heat is greater compared to the sensible heat percentage at 1250 W/CP and 2500 W/CP.

$$R_{th_sat} = \frac{T_{case} - T_{sat}}{q} \tag{1}$$

To determine the exit vapor quality from the CLs, the power dissipated by the heater, volumetric flow rate, inlet pressure, and inlet temperature of the CL were utilized. At a full load of 10 kW per CL, the maximum vapor quality recorded was 58%. Conversely, at a lower load of 1 kW per CL, the exit vapor quality was found to be 5%, indicating that 95% of the exiting refrigerant remained in the liquid phase. This phenomenon accounted for the higher thermal resistance observed at this load, as depicted in Fig. 11. The impact of exit quality on refrigerant thermal performance in the cold plates was analyzed using various correlations, where the results indicated that for qualities between 40 and 70%, the heat transfer coefficient is maximized, and lower values of case temperature and thermal resistance were noted [18].

An EES code was developed to design and evaluate the performance of CPs by calculating the two-phase Heat Transfer Coefficient (HTC) within the microchannels of the CP and the case temperature. This code incorporates three separate empirical correlations developed by Shah [26] eq (2), Gungor [27] eq (3), and Kandlikar [28] eq (4), as shown in Table 5. Additionally, it utilizes analytical methods to model the temperature distribution across various components of the CP. Subsequently, a user interface for the software was established. enabling users to input operational conditions and geometric parameters of the CP. This interface facilitates the prediction of temperature measurements at different points within the CPheater assembly, including the fin base, CP base, case temperature, and junction temperature. Fig. 12 displays the user interface of the developed code. Table 6 indicates that the experimental results demonstrated higher case temperatures compared to the correlations, suggesting that these correlations significantly overestimate the HTC. This discrepancy may stem from factors such as the manufacturability of the fins, surface flatness issues, and the thickness of the TIM.

Lastly, the P-h diagrams for the different thermal loads are displayed in Fig. 13, where the numbers indicate the cycle of the system: number 1 represents the refrigerant reservoir, 2 the CL inlet, 3 the CL outlet, and 4 the condenser inlet.

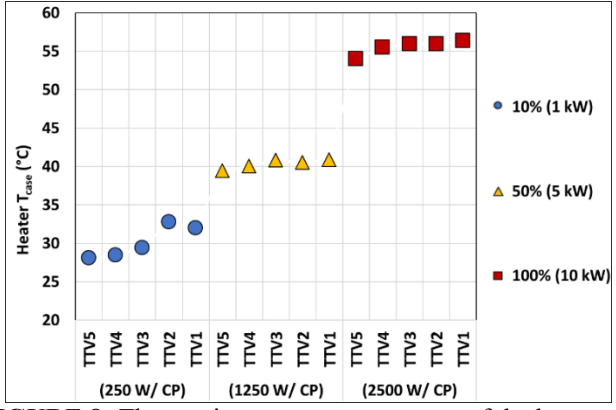


FIGURE 8: The maximum case temperature of the heaters in the TTVs with varying heat loads and constant flow rate.

Table 5: Flow boiling heat transfer correlations

$$h_{tp} = \frac{N_{u3}}{N_{u4}} \max(E, S) h_{sp}$$

$$h_{sp} = 0.023 (Re_f)^{0.8} (Pr_f)^{0.4} \frac{k_f}{d_h}$$

• For
$$NN > 1.0$$
,
 $S = \frac{1.8}{NN^{0.8}}$, $E = 230Bo^{0.5}$ (if $Bo > 3 \times 10^{-5}$)
Or, $E = 1 + 46Bo^{0.5}$ (if $Bo < 3 \times 10^{-5}$)

• For $0.1 < NN \le 1.0$,

$$S = \frac{1.8}{NN^{0.8}}, E = F B0^{0.5} \exp(2.74NN^{-0.1})$$

$$S = \frac{1.8}{NN^{0.8}}, E = F Bo^{0.5} \exp(2.47NN^{-0.15})$$

$$F = 14.7 \text{ (if } Bo \ge 11 \times 10^{-4})$$

$$Or, F = 15.43 \text{ (if } Bo < 11 \times 10^{-4})$$
(2)

If $Fr_f \ge 0.04$,

$$NN = Co$$

If $Fr_f < 0.04$,

$$NN = 0.38 \text{Fr}_f^{-0.3} \text{Co}$$

$$Co = \left(\frac{1 - x_e}{x_e}\right)^{0.8} \left(\frac{v_f}{v_g}\right)^{0.5}$$

where,

$$Fr_{\rm f} = \frac{v_{\rm f}^2 G^2}{g d_{\rm h}}$$

$$h_{\rm tp} = \frac{Nu_3}{Nu_4} (Eh_{\rm sp} + Sh_{\rm nb})$$

$$h_{\rm sp} = 0.023 ({\rm Re_f})^{0.8} ({\rm Pr_f})^{0.4} \frac{k_{\rm f}}{d_{\rm h}}$$

$$E = 1 + 24000 Bo^{1.16} + 1.37 \left(\frac{1}{X_{\rm tt}}\right)^{0.86}$$

$$h_{\rm nb} = 55 P_{\rm r}^{0.12} (-\log_{10}(P_{\rm r}))^{-0.55} M_{\rm W}^{-0.5} q_{\rm ch}^{\prime\prime 0.67}$$

$$S = (1 + 1.15 \times 10^{-6} E^2 Re_{\rm f}^{1.17})^{-1}$$
If $Fr_{\rm f} \le 0.05$, replace E by
$$EFr_{\rm f}^{0.1-2Fr_{\rm f}}$$
and S by $SFr_{\rm f}^{0.5}$, respectively

$$h_{\rm tp} = \frac{Nu_3}{Nu_4} \max(E, S) h_{\rm sp}$$

$$h_{\rm sp} = 0.023 (Re_{\rm f})^{0.8} (Pr_{\rm f})^{0.4} \frac{k_{\rm f}}{d_{\rm h}}$$

$$E = 0.6683 Co^{-0.2} f(Fr_{\rm f}) + 1058 Bo^{0.7}$$

$$S = 1.136 Co^{-0.9} f(Fr_{\rm f}) + 667.2 Bo^{0.7}$$

$$f(Fr_{\rm f}) = 1 (Fr_{\rm f} \ge 0.04)$$
Or,
$$f(Fr_{\rm f}) = (25 Fr_{\rm f})^{0.3} (Fr_{\rm f} < 0.04)$$

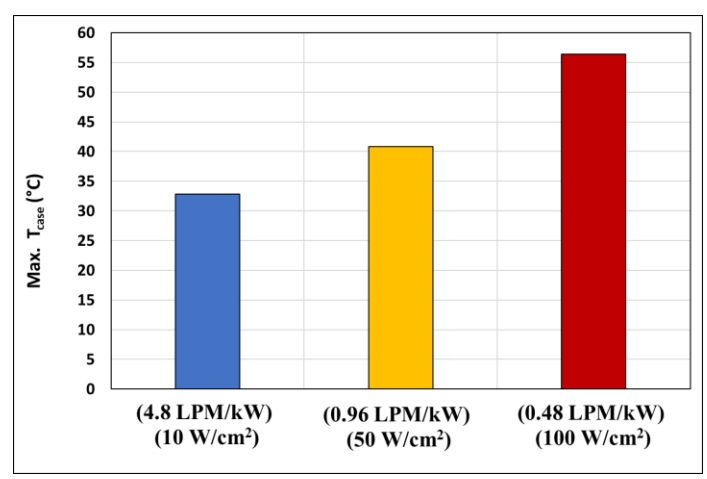


FIGURE 9: The maximum case temperature observed for the heaters with varying heat loads and constant flow rate.

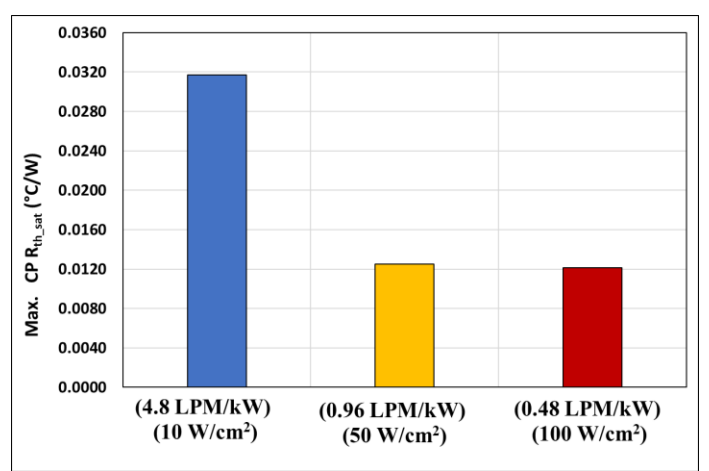


FIGURE 10: The maximum thermal resistance calculated of the cold plates with varying heat loads and constant flow rate.

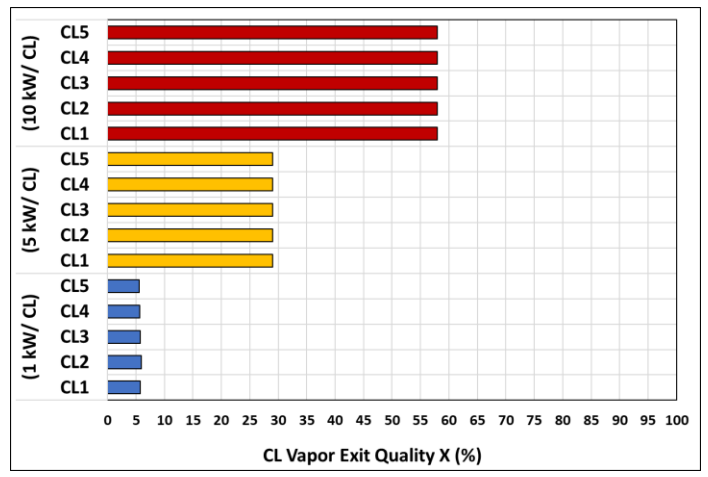
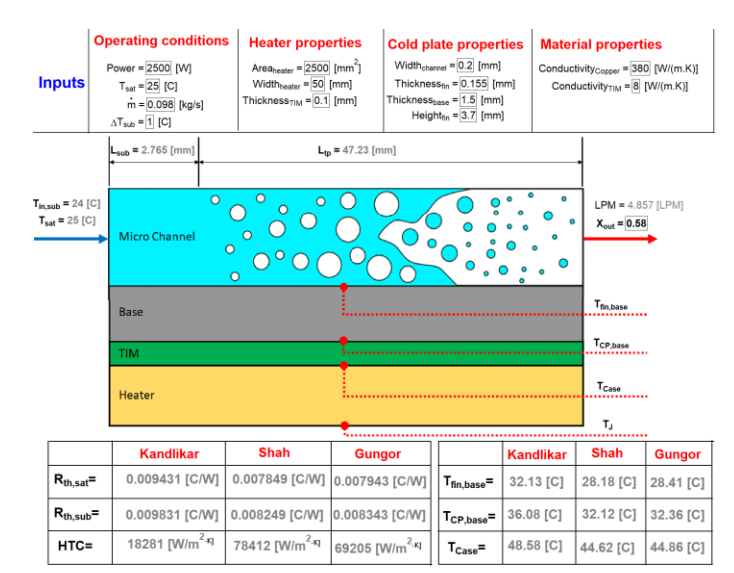


FIGURE 11: The vapor exits quality of the CLs with varying heat loads and constant flow rate.



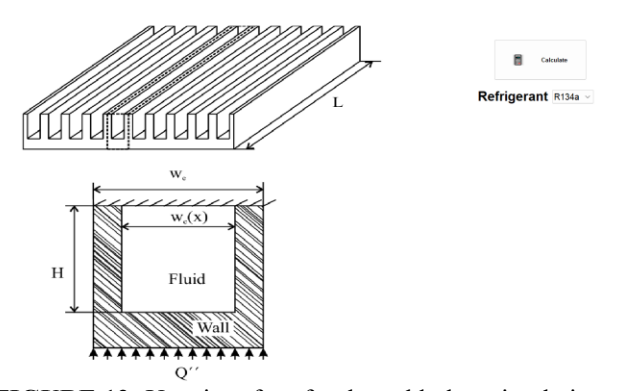


FIGURE 12: User interface for the cold plate simulation code

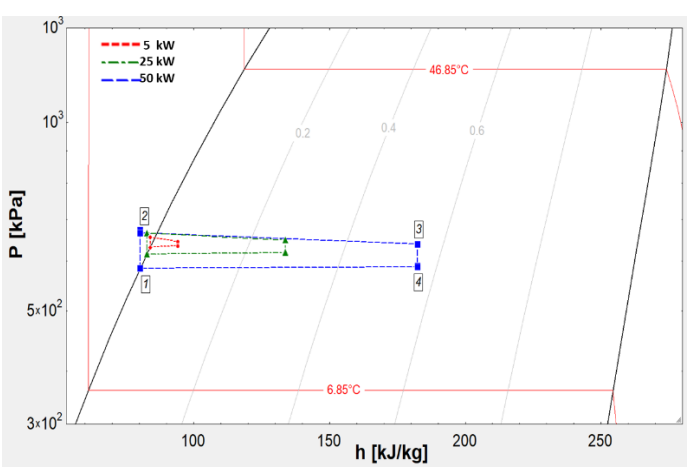


FIGURE 13: P-h diagram for the case studies.

Table 6: Flow boiling heat transfer correlations results

a (laW/ Dools)	Shah Gungor		Kandlikar
q (kW/ Rack)	[26]	[27]	[28]

5	HTC (W/m ² .K)	10762	17617	18028
	T _{case} (°C)	27.61	27.37	27.36
25	HTC (W/m ² .K)	34379	57097	46394
	T _{case} (°C)	35.74	35.12	35.36
50	HTC (W/m ² .K)	53397	68950	49670
	T _{case} (°C)	45.39	44.86	45.56

4.3 Uncertainty analysis

Uncertainty analysis, an essential step in experimental research, is conducted to evaluate and convey the accuracy and reliability of results. This analysis quantifies the inherent variability and errors present in each measurement, providing a deeper understanding of the data. Equations (5 and 6) illustrate the collective uncertainty derived from the uncertainties associated with each variable in the equation [29].

$$r = r(X_1, X_2, X_3, ... X_n)$$
(5)

$$\begin{split} \frac{U_r^2}{r^2} &= \left(\frac{X_1}{r} \frac{\partial r}{\partial X_1}\right)^2 \left(\frac{U_{X_1}}{X_1}\right)^2 + \left(\frac{X_2}{r} \frac{\partial r}{\partial X_2}\right)^2 \left(\frac{U_{X_2}}{X_2}\right)^2 + \cdots \\ &\quad + \left(\frac{X_n}{r} \frac{\partial r}{\partial X_n}\right)^2 \left(\frac{U_{X_n}}{X_n}\right)^2 \end{split} \tag{6}$$

$$\frac{U_{h_2}^2}{h_2^2} = \left(\frac{q}{h_2}\frac{\partial h_2}{\partial q}\right)^2 \left(\frac{U_q}{q}\right)^2 + \left(\frac{\dot{m}}{h_2}\frac{\partial h_2}{\partial \dot{m}}\right)^2 \left(\frac{U_{\dot{m}}}{\dot{m}}\right)^2 + \left(\frac{h_1}{h_2}\frac{\partial h_2}{\partial h_1}\right)^2 \left(\frac{U_{h_1}}{h_1}\right)^2 \tag{7}$$

In this equation, r is a function of J measured variables X, and U_{X_i} are the uncertainties in the measured variables, such as thermal resistance. Thermal resistance itself is dependent on factors like case temperature, refrigerant saturation inlet temperature, and total power. Moreover, equation (7) was used to calculate the uncertainties of the exit vapor quality. Table 6 displays all the uncertainties associated with the calculated values in the previous sections where an EES code was used for the calculations.

Table 6: Uncertainties of the calculated parameters.

Itama	Unit	Uncertainty at		
Items		50kW	25kW	5kW
Thermal resistance	°C/W	±0.0002	±0.0005	±0.002
Exit vapor quality	-	$\pm 1.83\%$	$\pm 0.89\%$	$\pm 0.59\%$

5. CONCLUSION

This study presents an innovative experimental framework designed to evaluate the feasibility of incorporating the development and testing of a two-phase, direct-to-chip cold plate liquid cooling system, specifically engineered for high-heat-density data centers and utilizing a P2P CDU at the rack level using a facility chilled water on the CDU's condenser. The key outcomes of this study are summarized as follows:

- Initially, the system's construction and assembly were outlined, following the commissioning process. Detailed descriptions of system components were provided, along with recommendations for best practices to ensure optimal functionality. Special emphasis was placed on the importance of filtration and maintaining the system free from any contamination.
- The hydraulic test of the system was conducted at a constant RST of 22°C, with varying flow rates. It was observed that the row manifold demonstrated good performance in terms of pressure drop. In contrast, as the volumetric flow rate increased to 36 LPM per rack, higher pressure drops were recorded on the rack manifold and the CLs. Specifically, the maximum pressure drops noted were 0.23 psi for the row manifold, 2.1 psi for the rack manifold, and 11.4 psi for the CLs, respectively. However, these pressure drops were significantly reduced at lower flow rates. The high pressure drops in the rack manifold and the CLs were attributed to the QDs size in the rack manifold, and the flow regulators and QDs size in the CLs. Further studies will be conducted to examine the pressure drops across the QDs and flow regulators separately.
- Subsequently, a thermal test was conducted with varying heat loads, reaching a maximum of 50 kW per rack, while maintaining a constant flow rate of 24 LPM/rack. In summary, the following maximum values were observed and measured at a specific rate of 0.48 LPM/kW (100 W/cm²):
 - The maximum ΔP_{return}, from the CL outlet to the condenser inlet, was recorded at 7.9 psi, and the ΔT_{sub} was maintained below -1.9°C. This value was influenced by the pressure drop on the return side. To address this issue, increasing the size of pipes and QDs on the return side could be a possible solution.
 - \circ The maximum heater case temperature T_{case} reached 56.4°C, the maximum saturation temperature T_{sat} was noted at

- 26°C, and the maximum vapor exit quality X from the CL was 58%.
- Furthermore, the maximum value for the CP thermal resistance at the saturation R_{th_sat} temperature was calculated to be 0.012°C/W.

REFERENCES

- [1] Sauciuc, L., Greg Chrysler, Ravi Mahajan, and Michele Szleper. "Air-cooling extension-performance limits for processor cooling applications." In Ninteenth Annual IEEE Semiconductor Thermal Measurement and Management Symposium, 2003., pp. 74-81. IEEE, 2003.
- [2] Zhang, H. Y., D. Pinjala, and Poi-Siong Teo. "Thermal management of high power dissipation electronic packages: From air cooling to liquid cooling." In *Proceedings of the 5th Electronics Packaging Technology Conference (EPTC 2003)*, pp. 620-625. IEEE, 2003.
- [3] J. Dai, M. M. Ohadi, D. Das, and M. G. Pecht, "Optimum cooling of data centers: Application of risk assessment and mitigation techniques," *Optimum Cooling of Data Centers: Application of Risk Assessment and Mitigation Techniques*, pp. 1–186, Jan. 2014, doi: 10.1007/978-1-4614-5602-5/COVER.
- [4] A. R. Gharaibeh, Y. M. Manaserh, M. I. Tradat, F. W. AlShatnawi, S. N. Schiffres, and B. G. Sammakia, "Using a Multi-Inlet/Outlet Manifold to Improve Heat Transfer and Flow Distribution of a Pin Fin Heat Sink," *J Electron Packag*, vol. 144, no. 3, Sep. 2022, doi: 10.1115/1.4054461.
- [5] Heydari, Ali, Ahmad R. Gharaibeh, Mohammad Tradat, Yaman Manaserh, Vahideh Radmard, Bahareh Eslami, Jeremy Rodriguez, and Bahgat Sammakia. "Experimental evaluation of direct-to-chip cold plate liquid cooling for high-heat-density data centers." Applied Thermal Engineering 239 (2024): 122122.
- [6] M. K. Sung and I. Mudawar, "Single-Phase and two-phase hybrid cooling schemes for high-heat-flux thermal management of defense electronics," *Journal of Electronic Packaging, Transactions of the ASME*, vol. 131, no. 2, pp. 0210131–02101310, Jun. 2009, doi: 10.1115/1.3111253/466145.
- [7] C. H. Hoang *et al.*, "Impact of fin geometry and surface roughness on performance of an impingement two-phase cooling heat sink," *Appl Therm Eng*, vol. 198, p. 117453, Nov. 2021, doi: 10.1016/J.APPLTHERMALENG.2021.117453.
- [8] Heydari, Ali, Yaman Manaserh, Ahmad Abubakar, Carol Caceres, Harold Miyamura, Alfonso Ortega, and Jeremy Rodriguez. "Direct-to-Chip Two-Phase Cooling for High Heat Flux Processors." In *International Electronic Packaging Technical Conference and Exhibition*, vol.

- 86557, p. V001T01A003. American Society of Mechanical Engineers, 2022.
- [9] Kwon B, Maniscalco NI, Jacobi AM, King WP. High power density two-phase cooling in microchannel heat exchangers. Applied Thermal Engineering. 2019;148:1271-7.
- [10] Lee J, Mudawar I. Two-phase flow in high-heat-flux micro-channel heat sink for refrigeration cooling applications: Part I—pressure drop characteristics. International Journal of Heat and Mass Transfer. 2005;48:928-40
- [11] Thiangtham P, Keepaiboon C, Kiatpachai P, Asirvatham LG, Mahian O, Dalkilic AS, et al. An experimental study on two-phase flow patterns and heat transfer characteristics during boiling of R134a flowing through a multimicrochannel heat sink. International Journal of Heat and Mass Transfer. 2016;98:390-400.
- [12] Lee J, Mudawar I. Two-phase flow in high-heat-flux micro-channel heat sink for refrigeration cooling applications: Part I—pressure drop characteristics. International Journal of Heat and Mass Transfer. 2005;48:928-40.
- [13] Lee J, Mudawar I. Two-phase flow in high-heat-flux micro-channel heat sink for refrigeration cooling applications: Part II—heat transfer characteristics. International Journal of Heat and Mass Transfer. 2005;48:941-55.
- [14] Lee J, Mudawar I. Low-Temperature Two-Phase Microchannel Cooling for High-Heat-Flux Thermal Management of Defense Electronics. IEEE Transactions on Components and Packaging Technologies. 2009;32:453-65
- [15] Bertsch SS, Groll EA, Garimella SV. Effects of heat flux, mass flux, vapor quality, and saturation temperature on flow boiling heat transfer in microchannels. International Journal of Multiphase Flow. 2009;35:142-54
- [16] Heydari, Ali, Yaman Manaserh, Ahmad Abubakar, Carol Caceres, Harold Miyamura, Alfonso Ortega, and Jeremy Rodriguez. "Direct-to-Chip Two-Phase Cooling for High Heat Flux Processors." In *International Electronic Packaging Technical Conference and Exhibition*, vol. 86557, p. V001T01A003. American Society of Mechanical Engineers, 2022.
- [17] Heydari, Ali, Yaman Manaserh, Mehdi Mehrabi, Ahmad Abubakar, Bahareh Eslami, Harold Miyamura, Alfonso Ortega, and Jeremy Rodriguez. "Refrigerant to Air Cooling for High Heat Density Two-Phase Cooled Data Centers." In 2023 22nd IEEE Intersociety Conference on Thermal and Thermomechanical Phenomena in Electronic Systems (ITherm), pp. 1-7. IEEE, 2023.
- [18] Heydari, Ali, Yaman Manaserh, Ahmad Abubakar, Harold Miyamura, Alfonso Ortega, and Jeremy Rodriguez. "Controlling Flow Instabilities in Direct-to-Chip Two-Phase Cooling for High Heat Flux Processors." In 2023 39th Semiconductor Thermal

- Measurement, Modeling & Management Symposium (SEMI-THERM), pp. 1-7. IEEE, 2023.
- [19] Layer, Ozone. "Montreal Protocol on Substances that Deplete the Ozone Layer Final Act 1987." (1988).
- [20] Protocol, Kyoto. "Framework convention on climate change." Kyoto Protocol (2010).
- [21] IPPC, Climate Change. "The Scientific Basis." (2001).
- [22] Calm, James M. "The next generation of refrigerants— Historical review, considerations, and outlook." international Journal of Refrigeration 31.7 (2008): 1123-1133.
- [23] Bansal, Pradeep, Edward Vineyard, and Omar Abdelaziz. "Advances in household appliances-A review." Applied Thermal Engineering 31.17-18 (2011): 3748-3760.
- [24] McLinden, Mark O., et al. "A thermodynamic analysis of refrigerants: Possibilities and tradeoffs for Low-GWP refrigerants." International Journal of Refrigeration 38 (2014): 80-92.
- [25] Heydari, Ali, Omar Al-Zu'bi, Yaman Manaserh, Mehdi Mehrabi, Farzaneh Hosseini, and Bahgat Sammakia. "

- System-Level Assessment of Green Refrigerant Replacements for Direct-to-Chip Two-Phase Cooling." In 2024 23rd IEEE Intersociety Conference on Thermal and Thermomechanical Phenomena in Electronic Systems (ITherm)(accepted).
- [26] Shah, M. Mohammed. "Chart correlation for saturated boiling heat transfer: equations and further study." ASHRAE Trans.;(United States) 88, no. CONF-820112-(1982).
- [27] Gungor, Kernal Ersin, and R. H. S. Winterton. "A general correlation for flow boiling in tubes and annuli." International Journal of Heat and Mass Transfer 29, no. 3 (1986): 351-358.
- [28] Kandlikar, Satish G. "A general correlation for saturated two-phase flow boiling heat transfer inside horizontal and vertical tubes." (1990): 219-228.
- [29] Holman, Jack Philip. "Experimental methods for engineers eighth edition." (2021).